



Graphene/PANI hybrid film with enhanced thermal conductivity by in situ polymerization

Jie Miao¹ , Haoliang Li¹ , Hanxun Qiu¹ , Xian Wu¹ , and Junhe Yang^{1,*}

¹ School of Material Science and Engineering, University of Shanghai for Science and Technology, Shanghai 200093, China

Received: 20 December 2017

Accepted: 2 February 2018

Published online:

23 March 2018

© Springer Science+Business Media, LLC, part of Springer Nature 2018

ABSTRACT

Heat dissipation in time is essential for long-term reliability of electrical devices. Graphene, with superior thermal conductivity and excellent flexibility, exhibits a potential to substitute currently used graphite film for thermal management. In this work, a free-standing film with enhanced thermal conductivity and better flexibility was achieved by a facile and environmentally friendly in situ polymerization. The ‘molecular welding’ strategy was introduced for preparation of graphitized graphene oxide/polyaniline (gGO/PANI) hybrid film, and the uniformly distributed PANI, serving as a solder, connected adjacent graphene sheets and filled in air voids of GO films. Scanning electron microscopy, Fourier transform infrared spectroscopy, X-ray photoelectron spectroscopy, X-ray diffraction and Raman spectroscopy were used to determine the structure of PANI and the interaction between GO and PANI. The in-plane thermal conductivity of gGO/PANI film is enhanced by 38% to $1019.7 \pm 0.1 \text{ W m}^{-1} \text{ K}^{-1}$ with addition of 12 wt% PANI, compared with that of pristine gGO film. Besides, the gGO/PANI film shows better flexibility than gGO film after 180° bending for 500 times.

Introduction

With dramatic development of high-power portable devices and next-generation flexible electronic equipments, thermal management has become the key to long-term reliability [1–3]. The thermal conductivity of currently used commercial expanded graphite film is only of $100\text{--}700 \text{ W m}^{-1} \text{ K}^{-1}$ [2, 4], which can hardly meet the requirements for heat dissipation. Although commercial

graphitized polyimide film shows a superior thermal conductivity ($1000\text{--}1750 \text{ W m}^{-1} \text{ K}^{-1}$), the poor mechanical property has greatly restricted the application in lateral heat dissipation [5]. Therefore, it is of great significance to pursue an alternative material with superior thermal conductivity, low cost as well as excellent flexibility for heat dissipation.

Graphene, a monolayer of two-dimensional honeycomb allotrope of carbon, possesses prominent electrical conductivity of 7200 S cm^{-1} [6] and thermal

Jie Miao and Haoliang Li contributed equally to this work.

Address correspondence to E-mail: jhyang@usst.edu.cn

conductivity of $5300 \text{ W m}^{-1} \text{ K}^{-1}$ at room temperature [7]. These unique properties make graphene an alternative material to fabricate thermal conducting films for thermal management. Graphene oxide (GO), as an intermediate in preparing graphene by Hummers method, is regarded as the precursor to fabricate graphene-based materials due to its excellent dispersion in water or organic solvents. Elaborate studies regarding reduced graphene oxide films (rGOF) have been carried out recently. For instance, the graphene oxide film was reduced on Cu foils, resulting in a high thermal conductivity of $902 \text{ W m}^{-1} \text{ K}^{-1}$ [8]. Song et al. [9] reported that the annealed filtrated graphene oxide film exhibited an enhanced thermal conductivity of $1043.5 \text{ W m}^{-1} \text{ K}^{-1}$. Shen et al. [10] prepared thin graphene film with an excellent thermal conductivity of $1100 \text{ W m}^{-1} \text{ K}^{-1}$ after being annealed and graphitized at $2000 \text{ }^\circ\text{C}$.

The superior performances of these rGOFs could be ascribed to the removal of functional groups and restoration of defects in GO sheets during the annealing process at high temperature. But the thermal conductivity of these reduced rGOFs was not comparable with that of single-layer graphene. On one hand, small GO layers may stack disorderly during the process of forming GOF. It will create much interspace between layers to lower the density of films. On the other hand, after being annealed at a high temperature, the removal of oxygen-containing groups will leave many defects in the structure of rGOF [11, 12]. These may break off channels for phonon transmission and increase the extent of phonon scattering [13]. In this regard, Peng et al. [5] delivered a debris-free graphene film with superior thermal conductivity as well as excellent flexibility by using large GO sheets. Furthermore, our group has proposed a ‘molecular welding’ strategy to enlarge the grain size of GO sheets via direct solution blending of polyimide. The thermal conductivity of welded graphene film showed a considerable enhancement [14]. The ‘molecular welding’ or employment of debris-free graphene sheets greatly enhanced the in-plane thermal conductivity of graphene film, because of the reduction in grain boundaries and phonon scattering.

Polyaniline (PANI) has already attracted a lot of research interests especially in supercapacitor, flexible electrodes and sensors [15–17], due to its excellent electroconductivity. However, there are few researches about the application of PANI in thermal

conductivity films. On one hand, PANI can be easily polymerized on GO in water [18, 19]. On the other hand, PANI provides sufficient active sites to interact with the functional groups in GO via covalent bonding or π - π interaction [20, 21]. Therefore, PANI was introduced as a solder to enlarge the size of rGO sheets and to repair defects of rGO film.

Herein, we put forward a more facile and environment friendly method to improve the thermal conductivity and flexibility of graphene film. The graphitized graphene oxide/PANI (gGO/PANI) hybrid films were fabricated via in situ polymerization in water. The introduction of PANI, as a solder, could strongly interact with GO via covalent bonding during the self-assembly process. After being heated at $2800 \text{ }^\circ\text{C}$, the PANI would weld adjacent small GO sheets and fill in intervals of GO sheets to enhance thermal conductivity and flexibility of films. The in-plane thermal conductivity of the optimized gGO/PANI film is superior to that of pristine graphene (gGO) film. Moreover, the gGO/PANI film survived in a 500 times bending test indicating a better flexibility.

Experiments

Materials

Pristine graphite powders (purity > 99.85%, particle size $\leq 30 \text{ }\mu\text{m}$), sulfuric acid (H_2SO_4 , 98 wt%), sodium nitrate, potassium permanganate (KMnO_4), hydrogen peroxide (H_2O_2 , 30 vol%), hydrochloric acid (HCl, 37 vol%), aniline and ammonium persulfate (APS) were purchased from National Pharmaceutical Group Chemical Co., Ltd.

Sample preparation

GO was prepared from natural graphite powders by a modified Hummers method. Briefly, graphite powders (5.0 g) and sodium nitrates (2.5 g) were added into concentrated sulfuric acid (115 mL) at room temperature. The mixture was put into an ice bath for 25 min under mild agitation, then potassium permanganate (15.0 g) was added slowly and kept the suspension’s temperature lower than $10 \text{ }^\circ\text{C}$ for another 25 min. The mixed suspension was then heated to $35 \text{ }^\circ\text{C}$ and kept for 45 min to form a thick paste. Deionized water (140 mL) was added and the temperature of the solution was kept at $98 \text{ }^\circ\text{C}$ for

another 45 min, the mixture turned from brown to yellow, and the mixture solution was diluted to 700 mL, then 30 mL H₂O₂ (30%) was added. The mixture was filtered and washed with 50 mL of HCl solution. Finally, the solution was centrifuged for several times at 11000 rpm until the pH of the system was about 7. The high-speed centrifuging (11000 rpm, 10 min) of GO suspension in water was carried out and treated in an ultrasonic cleaner (KQ-100, frequency 40 kHz, output power 100 W) for one hour. At last, a centrifuge of 3000 rpm, 15 min was used to separate excess unreacted graphite powder and the stable GO aqueous solution was ready for the preparation of GO/PANI.

In a typical process of preparing GO/PANI-12%, 0.024 mL aniline was firstly dispersed in 7 mL HCl solution with the help of bath sonication. Then, it was added into 40 mL GO solution (5 mg/mL) with stirring at temperature below 4 °C for 0.5 h. After that, 13 mL APS solution (1.8 mg/mL) was added into the mixed solution slowly. Under mild agitation for 4 h, as shown in Fig. S1, the color of the solution turned from brown to black. The dispersion was washed for several times until the pH of system was about 7 by centrifugation at 11000 rpm. Similarly, GO/PANI films with different amount of PANI were prepared, denominated as GO/PANI-*x*%, where *x* represented the weight percentage of PANI to GO (*X* = 10, 12, 14 and 16, respectively).

Carbonization and graphitization of GO and GO/PANI films

As illustrated in Fig. 1, the GO and GO/PANI dispersion were poured into the Teflon molds for self-assembly in dry oven at 60 °C for 6–10 h. The GO sheets were spontaneously assembled at the interface between the dispersion and the air to form a free-standing film. Then, the films were thermally reduced in a tube furnace at 800 °C for 1 h. After that, the GO and GO/PANI-*x*% films were graphitized at 2800 °C, denominating as gGO and gGO/PANI-*x*% films, respectively. Finally, cold pressing was performed with a rolling machine in order to make samples dense.

Characterization

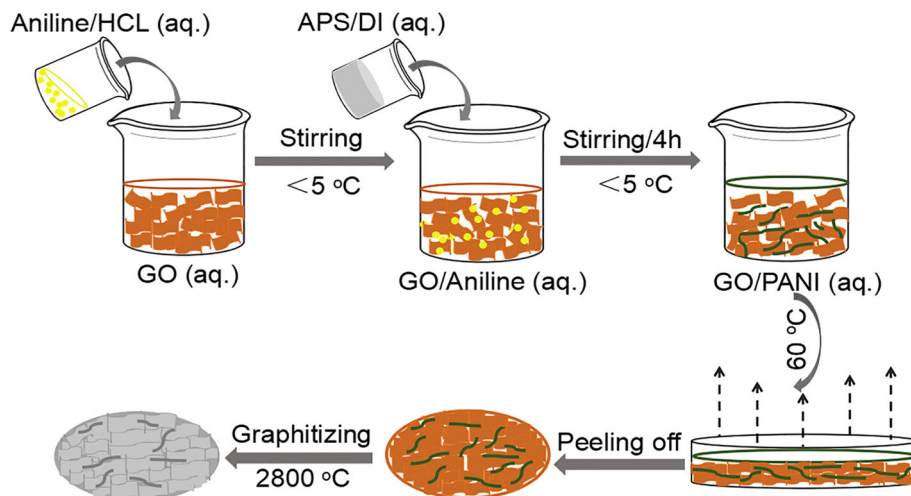
Surface and cross-sectional observations of GO and GO/PANI films were performed on scanning electron microscopy (SEM, FEI Quanta FEG) with an

accelerating voltage of 20 kV. Fourier transform infrared spectroscopy (FTIR, P.E. Spectrum 100) was collected on a spectrum from 400 to 4000 cm⁻¹. The X-ray photoelectron spectroscopy (XPS, Physical Electronics PHI 5000C ESCA) was carried out with a Sigma Probe and monochromatic X-ray source. The LabRAM spectrometer (Horiba, LabRAM HR Evolution, France) was used to analyze the structure of GO and GO/PANI film before and after graphitizing with a laser length of 532 nm. X-ray diffraction (XRD, Bruker D8 ADVANCE) patterns were measured using Cu K α (λ = 0.154 nm) radiation with a generator voltage of 40 kV and a current of 40 mA. Thermal gravimetric analysis (TGA) was performed under N₂ atmosphere using a PerkinElmer thermogravimetric analyzer. The thermal diffusivity (α) of gGO and gGO/PANI thin films was measured using a laser flash method (LFA 467/Ins Nanoflash, Entsch) at room temperature. The thermal conductivity (*k*) was calculated according to ASTM E 1461-92 standard method using the equation: $k = \alpha \times C_p \times \rho$, where *C_p* and ρ represented the specific heat capacity and the density of samples, respectively. The *C_p* was determined by a differential scanning calorimetry (DSC 200F3, Netzsch) from -20 °C to 120 °C. The electrical conductivities of gGO and gGO/PANI films were measured by four-point probe method (RTS-9, Scientific Equipment and Services) at room temperature.

Results and discussion

Figure 2 SEM presents the surface and cross-sectional morphologies of GO, GO/PANI-12% films. As shown in Fig. 2a, pristine GO film shows an integrated surface morphology and many ripples. While the surface morphology of GO/PANI-12% film in Fig. 2c is less rough, the EDX mapping of GO/PANI-12% film in Fig. S2b–d indicates the uniform distribution of PANI on surface of GO/PANI-12% film. It can be seen from the cross section of GO film in Fig. 2b that GO sheets stacks up to form a layered structure with many disordered wrinkles. However, the cross section of GO/PANI-12% film (Fig. 2d) displays a more highly aligned structure. In the inset, compared to the pristine GO film, there are some particles attached on both the surface and cross section of GO/PANI-12% film, indicating the presence of PANI in the interlayers of sample. It is worth noting that the

Figure 1 Schematic diagram of the fabrication of the gGO and gGO/PANI-x% films.



morphology of PANI is in accordance with reported [16]. Figure 2f exhibits the cross section of GO/PANI-16% film and the layered structure of GO/PANI-16% film is covered by excessive PANI. The agglomeration of PANI would hamper the self-assembly to form a layered structure and result in a higher extent of defects.

FTIR spectra were used to determine the successful polymerization of PANI and the reaction between GO and PANI (Fig. 3). The adsorption peaks of GO film located at 1751 and 1054 cm^{-1} are assigned to the C=O bending vibration in -COOH groups and C-O-C stretching [22, 23], respectively. The typical peaks of PANI appearing at 1569 , 1487 , 1309 , 1245 and 1142 cm^{-1} are attributed to C=C stretching vibration of quinoid ring, C=C stretching of benzene ring, C-N stretching of secondary aromatic amines, C-H bonds of the benzenoid ring and the quinoid ring [15, 24, 25], respectively. All characteristic peaks of GO and PANI can be observed in GO/PANI hybrid film (remained at $120\text{ }^\circ\text{C}$ for 1 h). Moreover, two additional peaks at 1650 and 3113 cm^{-1} in GO/PANI- $120\text{ }^\circ\text{C}$ film assigned to C=O in -CONH (amide I) stretching bands and N-H stretching bands [26] imply that GO and PANI has an interaction via covalent bonding, proving the successful in situ synthesis of PANI in GO.

In order to verify the reaction between GO and PANI, XPS spectroscopy was further employed. As shown in Fig. 4, the C 1s spectra of GO can be divided into five components, corresponding to non-oxygenated carbon ring C=C (284.7 eV), sp^3 hybridization of C (285.5 eV), epoxy carbon (286.9 eV) [27], carbonyl carbon (287.6 eV) and

carboxylic acid carbon (288.9 eV), respectively [28]. In comparison with GO, the C 1s of GO/PANI-12% after being heated at $120\text{ }^\circ\text{C}$ for 1 h in Fig. 4b has an additional peak (C-N) at 285.9 eV [29]. It implies that PANI has been successfully obtained. The area of C=O in GO/PANI becomes larger than that of GO (17.85 vs. 15.72%), while -COOH in GO/PANI smaller than GO (1.06 vs. 2.02%). The changes of proportions of C=O and -COOH indicate the transformation of -COOH into -NHCO, verifying the reaction between GO and PANI. Figure 4c shows N 1s core-level spectra of PANI. The N 1s peaks at 399.2 , 399.7 and 401.7 eV are attributed to -N=, -NH- and -N⁺ species, respectively [30]. The N 1s spectra of GO/PANI- $120\text{ }^\circ\text{C}$ are shown in Fig. 4d and the spectra include -N= at 399.2 eV , -NH₂ at 399.7 eV , -NHC=O at 400.2 eV and -N⁺ at 401.7 eV [28]. The decreasing area of -NH- peak and the existence of new -NH-C=O peak could be both associated with the reaction between -NH₂ of PANI and -COOH of GO. Both the results of FTIR and XPS can prove the occurrence of reactions and covalent interaction between GO and PANI.

The XRD patterns of GO and GO/PANI films before and after graphitization are conducted as displayed in Fig. 5. The detailed information about peak position (2θ), $d_{(001)}$ and $d_{(002)}$ of each sample before and after graphitization is listed in Table S1. In Fig. 5a, the peak position of GO is 10.90° , and with the increase in PANI amount, the peak position has a slight shift to 10.70° . According to the Bragg's equation, $d_{(001)}$ changes from 0.8107 to 0.8258 nm . The results indicate the successful insertion of PANI into interlayers of GO film. As shown in Fig. 5b, peak

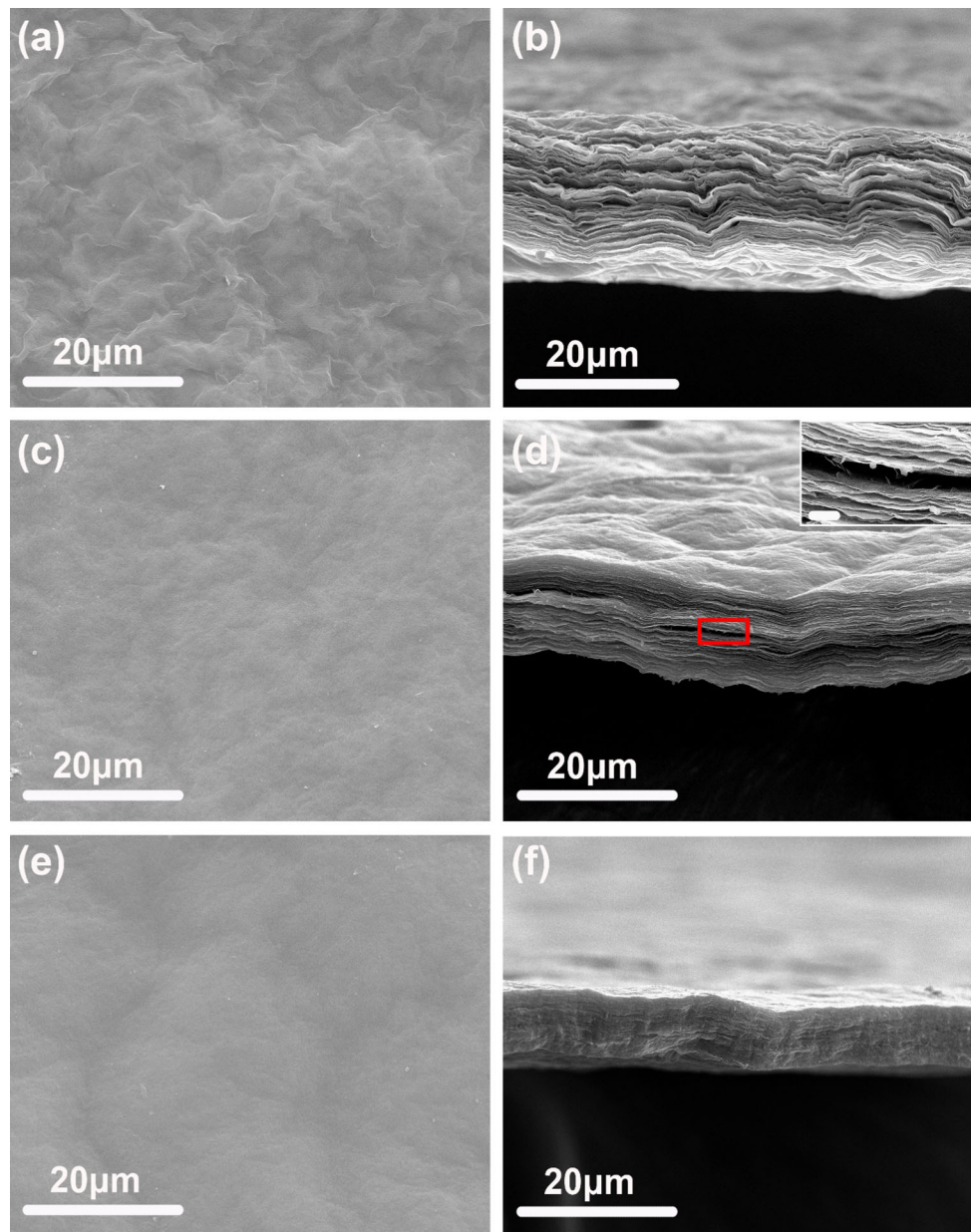


Figure 2 SEM images of the surface of GO film (a), GO/PANI-12% film (c) and GO/PANI-16% film (e); cross section of GO film (b), GO/PANI-12% film (d) and GO/PANI-16% film (f). The inset shows the magnification of the selected area and the scale bar is 1 μm .

position of gGO film shifts to 26.50° , corresponding to a $d_{(002)}$ spacing of 0.3360. With the increase in PANI, the 2θ shows a slight increase firstly. Notably, the $d_{(002)}$ spacing of gGO/PANI-12% is the minimum ($2\theta = 26.54$, $d = 0.3357$ nm), which is closest to the pristine graphite ($d = 0.3354$ nm) [31, 32]. But with increased addition of PANI, the 2θ peak shifts to 26.5° , corresponding to a $d_{(002)}$ spacing of 0.3360. The results reveal that the intercalated PANI can weld small GO sheet to enlarge its grain size and fill the voids in GO/PANI films during graphitization

treatment. While excessive PANI (GO/PANI-16%) tends to aggregate among GO layers, which will increase the interlayer space and thermal resistance. The results of XRD are in accordance with SEM.

Raman spectroscopy was used to investigate the structure of GO and GO/PANI hybrid films before and after graphitization (Fig. 6). Two main characteristic bands can be seen, corresponding to D-band at ~ 1300 cm^{-1} [33] and G-band at ~ 1580 cm^{-1} [34], respectively. The D-band and G-band usually assign to K-point phonons of A_{1g} symmetry and zone

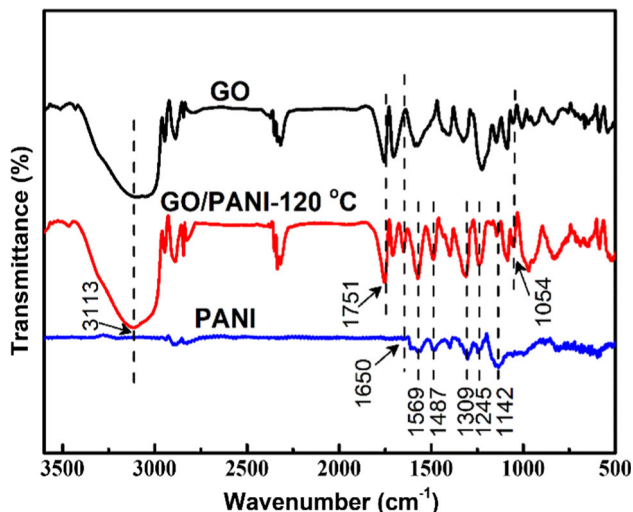


Figure 3 FT-IR spectra of GO film, GO/PANI-120 °C hybrid film and the pristine PANI.

center phonons of E_{2g} symmetry [21]. I_D/I_G was usually to present the degree of inferiority of

material. The detailed information of I_D/I_G of each sample is listed in Table S2. With increase in PANI amount, the I_D/I_G of GO/PANI increases from 1.398 to 1.660, indicating that the presence of PANI in GO would lead to some defects in GO [35]. The I_D/I_G of GO/PANI-12% after graphitization, as displayed in Fig. 6b, is minimum (0.0600), which means the defects are the least and the degree of graphitization is the highest. While the Raman spectra of PANI after graphitization (in Fig. S3) suggest that PANI can be transformed into graphitic material still with some disordered structure. Therefore, the reasons of the decreasing I_D/I_G of hybrid films lie in that the graphitized PANI serving as additional carbon source, could weld adjacent GO sheet and repair defects of GO, as reduce the phonon scattering and provide channels for phonon transportation. However, when PANI (GO/PANI-16%) is excessive, they may aggregate together to some extent and create more defects in GO film.

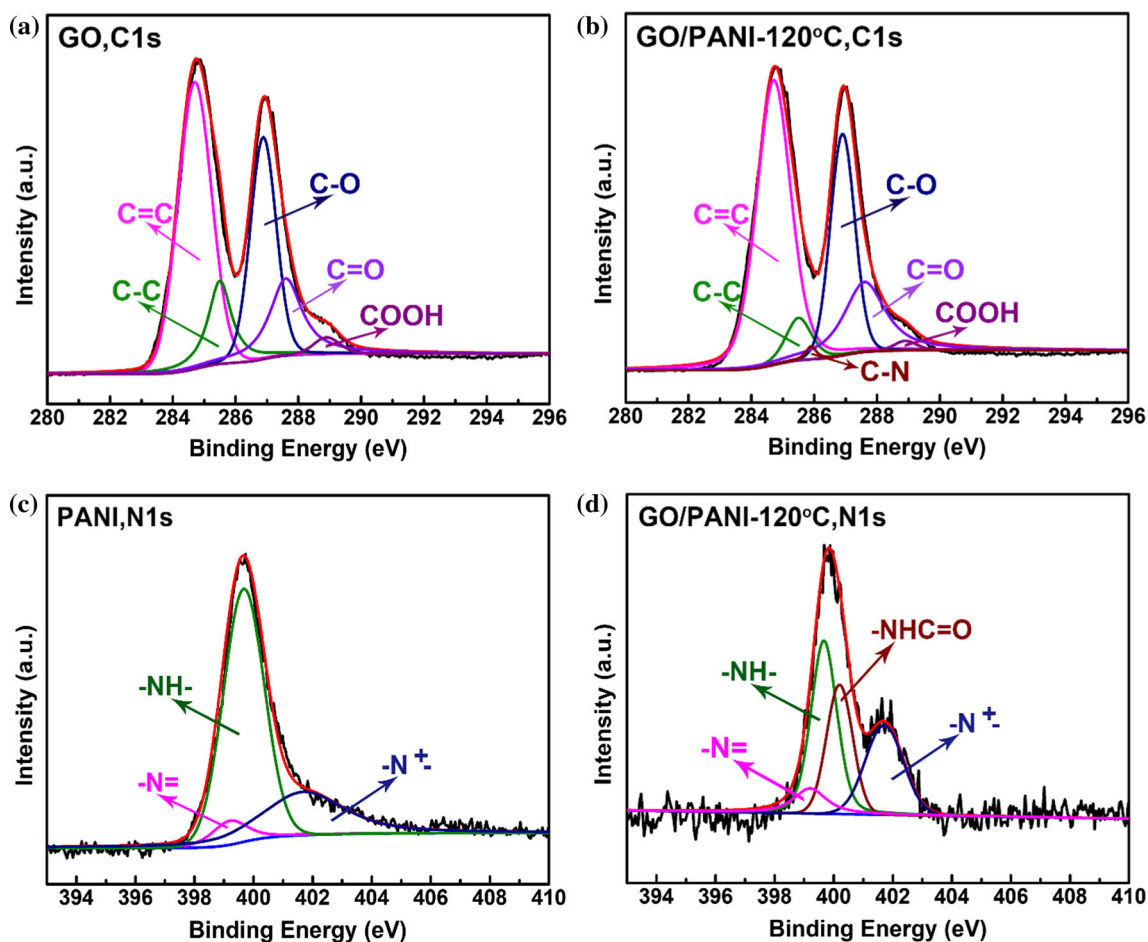


Figure 4 The deconvoluted spectra of C 1s of a GO, b GO/PANI-120 °C and N 1s of c GO, d GO/PANI.

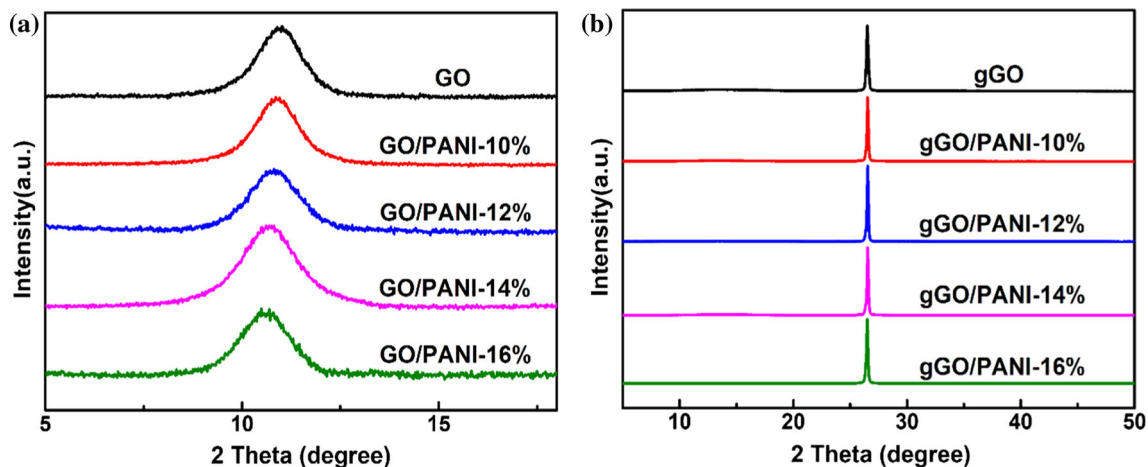


Figure 5 XRD patterns of **a** GO and GO/PANI films, **b** gGO and gGO/PANI films.

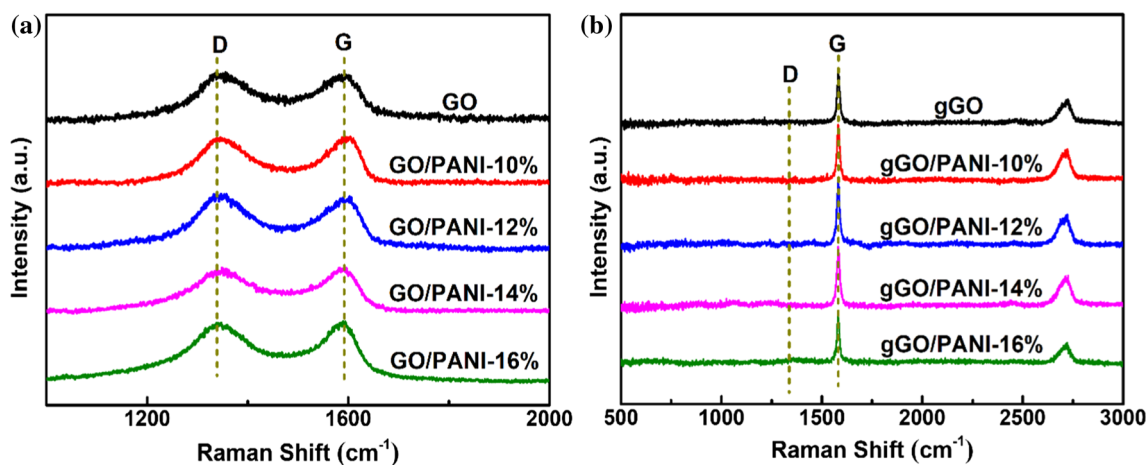


Figure 6 Raman spectra of **a** GO and GO/PANI films, **b** gGO and gGO/PANI films.

Figure 7 shows thermal gravimetric analysis (TGA) of GO, GO/PANI-12%, GO/PANI-16% film and PANI. The thermal stability of GO film is relatively poor which exhibits a major weight loss at 200 °C due to the thermal decomposition of oxygen-containing functional groups such as –OH, –CO and –COOH [19, 21]. The onset weight loss temperature of GO/PANI-12% is the same as pristine GO film, while that of GO/PANI-16% shifts to 180 °C. As commonly observed, the weight loss below 100 °C is due to the vaporization of water, and the rapid weight loss at 530 °C is attributed to the decomposition of PANI [36]. The thermal stability of GO/PANI-12% film and GO/PANI-16% film is remarkably enhanced due to the presence of PANI and the strong interaction between GO and PANI [37]. For instance, the GO/PANI-12% film and GO/PANI-16% film show 54.6 and 51.5% weight loss at 730 °C, while 62.2% weight

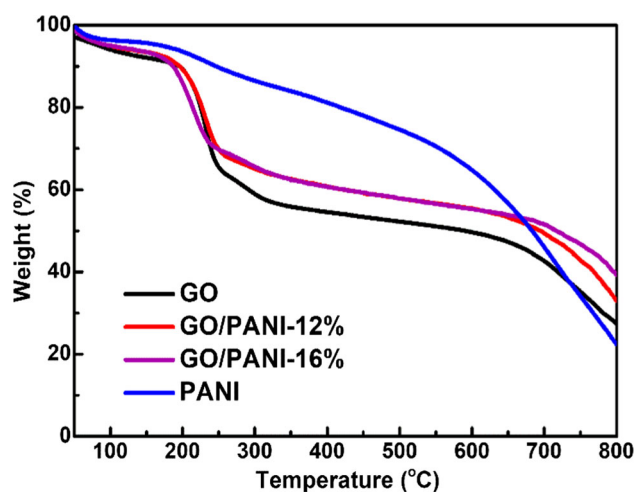


Figure 7 TGA thermograms of GO film, GO/PANI-12% film, GO/PANI-16% film and PANI powders at a rate of 5 °C/min.

loss occurs in GO film and pure PANI at the same temperature.

The in-plane thermal diffusivity of gGO/PANI hybrid films was measured by laser flash method, as shown in Fig. 8a. The thermal conductivity of gGO film is $738.2 \pm 6.3 \text{ Wm}^{-1} \text{ K}^{-1}$. With the increase in PANI, the thermal conductivity of gGO/PANI-12% film reaches the maximum of $1019.7 \pm 0.1 \text{ Wm}^{-1} \text{ K}^{-1}$, which has been improved by 38% compared with gGO film. The thermal conductivity of gGO/PANI-12% film is much higher than the well-aligned carbon nanotube arrays ($786.8 \pm 6.636 \text{ Wm}^{-1} \text{ K}^{-1}$) [38], the optimized graphene fibers (larger sized graphene sheets with 30 wt% small size graphene sheets, $K = 607 \pm 25 \text{ Wm}^{-1} \text{ K}^{-1}$) [39]. We also make a comparison with some thermal conducting materials reported recently as listed in Table S4. However, excessive PANI (GO/PANI-16%) would agglomerate between GO layers, leading to a dramatic decrease in in-plane thermal conductivity. To investigate the flexibility of hybrid films, a small-radius bending test was conducted as the inset showed, followed by the measurement of electrical resistivity (σ), as displayed in Fig. 8b. The fitted curve of I/I_0 ($I = \sigma^{-1}$) of gGO/PANI-12% film shows a gradual decrease to 0.85 after 500 times 180° bending. While, that of gGO film has an obvious reduction to 0.69, demonstrating that the inner structure of gGO film had a more obvious breakage. The results indicate that gGO/PANI-12% film exhibits better flexibility than gGO film. The reasons ascribed to

improvement might be that the added PANI after graphitization can weld adjacent GO sheet and turn into a part of film to repair defects of GO and make the hybrid film more compact.

The mechanism of PANI to improve the in-plane thermal conductivity and flexibility of gGO film is illustrated in Fig. 9. Firstly, GO provides sites for successful in situ polymerization of anilines. Then, as the ‘molecular welding’ strategy explained, added PANI improves the thermal conductivity and flexibility of gGO film through following two ways. One way is that the $-\text{NH}_2$ groups in PANI interacted with $-\text{COOH}$ in GO during the heating process by forming $-\text{NHCO}$ bonding. The intercalated PANI after graphitization treatment can be transformed into a kind of graphite material to weld the micron-sized GO sheets and reduce grain boundaries. The other is that PANI could serve as additional carbon sources to repair the defects and make the film with larger density after graphitization. Both the two ways can result in a less extent of phonon scattering and less thermal resistance.

Conclusion

In conclusion, a more facile and environmentally friendly method was employed for the successful preparation of GO/PANI hybrid film by in situ synthesis of PANI on GO. With 12 wt% addition of PANI, the in-plane thermal conductivity of gGO film

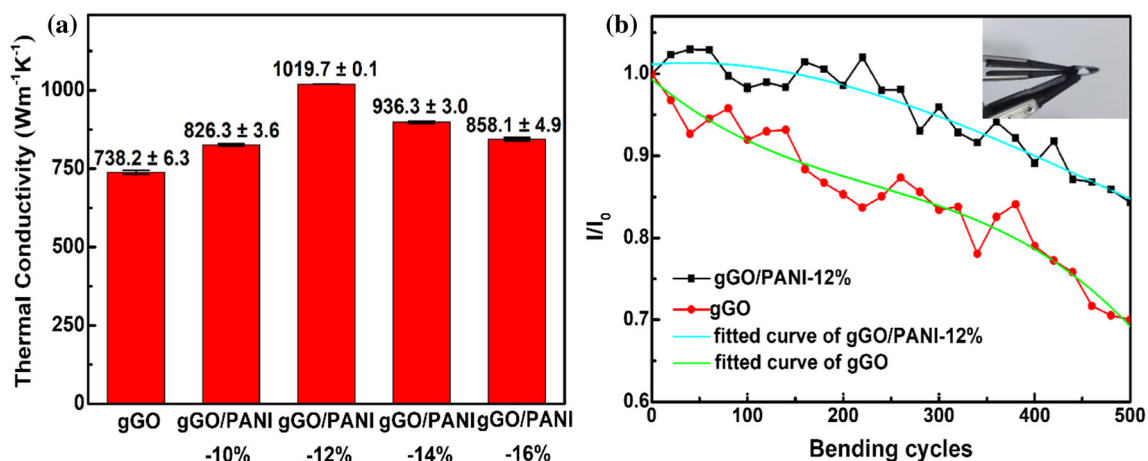


Figure 8 a Thermal conductivities of gGO and gGO/PANI film (the error bar represented the standard deviation. In the LFA measurement, each sample was spotted for three times).

b Electrical resistivity (σ , $I = \sigma^{-1}$) of gGO and gGO/PANI film after repeated 180° bending for 500 times (I_0 represented the electrical conductivity of each sample before bending).

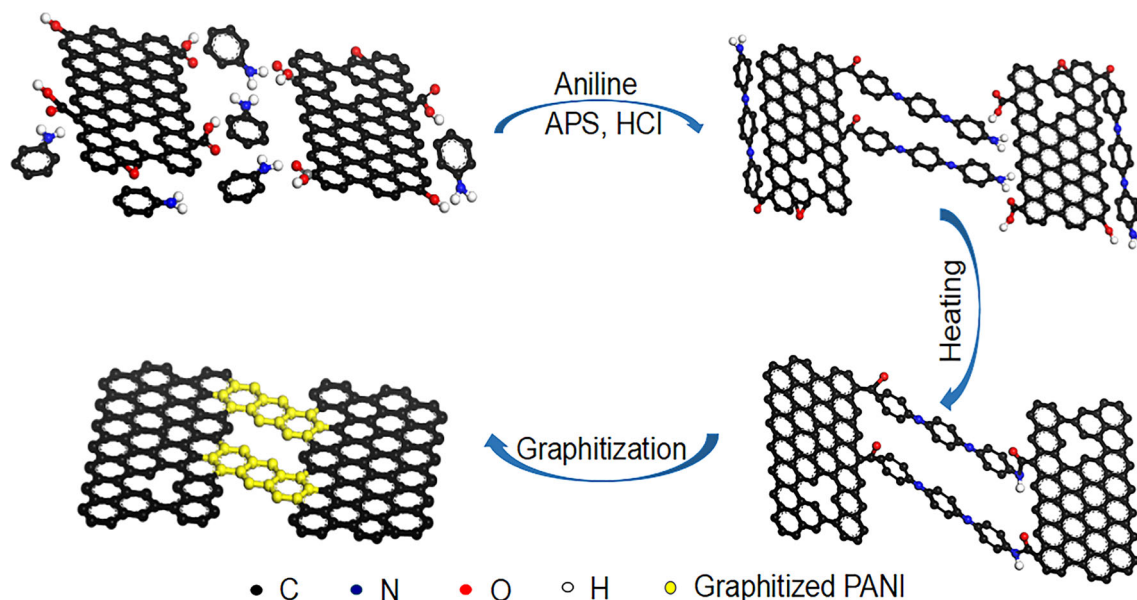


Figure 9 The mechanism of interaction between GO and PANI.

reached $1019.7 \pm 0.1 \text{ W m}^{-1} \text{ K}^{-1}$, which has an enhancement by 38% compared to the pristine gGO film. Furthermore, the flexibility of gGO/PANI-12% film was much better than gGO film after 180° bending for 500 times. The intercalated graphitized PANI, as a solder, could weld GO sheets via covalent bonding and provide carbon sources for the repair of defects in GO. We believe that a new method of preparation gGO/PANI hybrid film for improving thermal conductivity and flexibility of graphene films shows a great potential in heat dissipation for high-power electronic devices.

Acknowledgements

The authors are thankful to National Natural Science Foundation of China (51472160, E020603), Science and Technology Commission of Shanghai Municipality (15JC-1490700, 16JC1402200) and Shanghai Municipal Commission of Economy and Information Technology for their financial supports to this work.

Electronic supplementary material: The online version of this article (<https://doi.org/10.1007/s10853-018-2112-z>) contains supplementary material, which is available to authorized users.

References

- [1] Balandin AA (2011) Thermal properties of graphene, carbon nanotubes and nanostructured carbon materials. *Nat Mater* 10:569–581
- [2] Feng W, Qin M, Feng Y (2016) Toward highly thermally conductive all-carbon composites: structure control. *Carbon* 109:575–597
- [3] Warzoha RJ, Fleischer AS (2014) Heat flow at nanoparticle interfaces. *Nano Energy* 6:137–158
- [4] Wei XH, Liu L, Zhang JX, Shi JL, Guo QG (2010) Mechanical, electrical, thermal performances and structure characteristics of flexible graphite sheets. *J Mater Sci* 45:2449–2455. <https://doi.org/10.1007/s10853-010-4216-y>
- [5] Peng L, Xu Z, Liu Z, Guo Y, Li P, Gao C (2017) Ultrahigh thermal conductive yet superflexible graphene films. *Adv Mater* 29:1700589
- [6] Li D, Muller MB, Gilje S, Kaner RB, Wallace GG (2008) Processable aqueous dispersions of graphene nanosheets. *Nat Nanotechnol* 3:101–105
- [7] Balandin AA, Ghosh S, Bao W, Calizo I, Teweldebrhan D, Miao F, Lau CN (2008) Superior thermal conductivity of single-layer graphene. *Nano Lett* 8:902–977
- [8] Huang SY, Zhao B, Zhang K, Yuen MM, Xu JB, Fu XZ, Sun R, Wong CP (2015) Enhanced reduction of graphene oxide on recyclable Cu foils to fabricate graphene films with superior thermal conductivity. *Sci Rep* 5:14260
- [9] Song N-J, Chen C-M, Lu C, Liu Z, Kong Q-Q, Cai R (2014) Thermally reduced graphene oxide films as flexible lateral heat spreaders. *J Mater Chem A* 2:16563–16568

- [10] Shen B, Zhai W, Zheng W (2014) Ultrathin flexible graphene film: an excellent thermal conducting material with efficient EMI shielding. *Adv Funct Mater* 24:4542–4548
- [11] Chen C-M, Huang J-Q, Zhang Q, Gong W-Z, Yang Q-H, Wang M-Z, Yang Y-G (2012) Annealing a graphene oxide film to produce a free standing high conductive graphene film. *Carbon* 50:659–667
- [12] Vallés C, Núñez JD, Benito AM, Maser WK (2012) Flexible conductive graphene paper obtained by direct and gentle annealing of graphene oxide paper. *Carbon* 50:835–844
- [13] Kim JY, Lee JH, Grossman JC (2012) Thermal transport in functionalized graphene. *ACS Nano* 6:9050–9057
- [14] Li H, Dai S, Miao J, Wu X, Chandrasekharan N, Qiu H, Yang J (2018) Enhanced thermal conductivity of graphene/polyimide hybrid film via a novel “molecular welding” strategy. *Carbon*. <https://doi.org/10.1016/j.carbon.2017.10.044>
- [15] Meng Y, Wang K, Zhang Y, Wei Z (2013) Hierarchical porous graphene/polyaniline composite film with superior rate performance for flexible supercapacitors. *Adv Mater* 25:6985–6990
- [16] Kumar NA, Choi HJ, Shin YR, Chang DW, Dai L, Baek JB (2012) Polyaniline-grafted reduced graphene oxide for efficient electrochemical supercapacitors. *ACS Nano* 6:1715–1723
- [17] Zhang L, Wang W, Cheng J et al (2018) Skeleton networks of graphene wrapped double-layered polypyrrole/polyaniline nanotubes for supercapacitor applications. *J Mater Sci*. <https://doi.org/10.1007/s10853-017-1543-2>
- [18] Dhand C, Das M, Datta M, Malhotra BD (2011) Recent advances in polyaniline based biosensors. *Biosens Bioelectron* 26:2811–2821
- [19] Kong L-B, Zhang J, An J-J, Luo Y-C, Kang L (2008) MWNTs/PANI composite materials prepared by in situ chemical oxidative polymerization for supercapacitor electrode. *J Mater Sci* 43:3664–3669. <https://doi.org/10.1007/s10853-008-2586-1>
- [20] Tong Z, Yang Y, Wang J, Zhao J, Su B-L, Li Y (2014) Layered polyaniline/graphene film from sandwich-structured polyaniline/graphene/polyaniline nanosheets for high-performance pseudosupercapacitors. *J Mater Chem A* 2:4642–4651
- [21] Zengin H, Zhou W, Jin J, Czerw R, Smith DW, Echegoyen L, Carroll DL, Foulger SH, Ballato J (2002) Carbon nanotube doped polyaniline. *Adv Mater* 14:1480–1483
- [22] Mishra AK, Ramaprabhu S (2011) Functionalized graphene-based nanocomposites for supercapacitor application. *J Phys Chem C* 115:14006–14013
- [23] Olowojoba GB, Kopsidas S, Eslava S, Gutierrez ES, Kinloch AJ, Mattevi C, Rocha VG, Taylor AC (2017) A facile way to produce epoxy nanocomposites having excellent thermal conductivity with low contents of reduced graphene oxide. *J Mater Sci* 52:7323–7344. <https://doi.org/10.1007/s10853-017-0969-x>
- [24] Cong H-P, Ren X-C, Wang P, Yu S-H (2013) Flexible graphene–polyaniline composite paper for high-performance supercapacitor. *Energy Environ Sci* 6:1185
- [25] Konwer S (2016) Graphene oxide-polyaniline nanocomposites for high performance supercapacitor and their optical, electrical and electrochemical properties. *J Mater Sci: Mater Electron* 27:4139–4146
- [26] Luong ND, Hippi U, Korhonen JT, Soininen AJ, Ruokolainen J, Johansson L-S, Nam J-D, Sinh LH, Seppälä J (2011) Enhanced mechanical and electrical properties of polyimide film by graphene sheets via in situ polymerization. *Polymer* 52:5237–5242
- [27] Xue X, Yin Q, Jia H, Zhang X, Wen Y, Ji Q, Xu Z (2017) Enhancing mechanical and thermal properties of styrene-butadiene rubber/carboxylated acrylonitrile butadiene rubber blend by the usage of graphene oxide with diverse oxidation degrees. *Appl Surf Sci* 423:584–591
- [28] Zhang L-B, Wang J-Q, Wang H-G, Xu Y, Wang Z-F, Li Z-P, Mi Y-J, Yang S-R (2012) Preparation, mechanical and thermal properties of functionalized graphene/polyimide nanocomposites. *Compos Part A* 43:1537–1545
- [29] Tang Z, Zhang Z, Han Z, Shen S, Li J, Yang J (2016) One-step synthesis of hydrophobic-reduced graphene oxide and its oil/water separation performance. *J Mater Sci* 51:8791–8798. <https://doi.org/10.1007/s10853-016-9937-0>
- [30] Lu X, Li L, Song B, Moon K-S, Hu N, Liao G, Shi T, Wong C (2015) Mechanistic investigation of the graphene functionalization using p-phenylenediamine and its application for supercapacitors. *Nano Energy* 17:160–170
- [31] Ghosh T, Biswas C, Oh J, Arabale G, Hwang T, Luong ND, Jin M, Lee YH, Nam J-D (2012) Solution-processed graphite membrane from reassembled graphene oxide. *Chem Mater* 24:594–599
- [32] Zhang K, Zhang X, Li H, Xing X, Jin L, Cao Q, Li P (2017) Direct exfoliation of graphite into graphene in aqueous solution using a novel surfactant obtained from used engine oil. *J Mater Sci* 53:2484–2496. <https://doi.org/10.1007/s10853-017-1729-7>
- [33] Ferrari AC, Basko DM (2013) Raman spectroscopy as a versatile tool for studying the properties of graphene. *Nat Nanotechnol* 8:235–246
- [34] Zhu B, Deng Z, Yang W, Wang H, Gao L (2015) Pyrolyzed polyaniline and graphene nanosheet composite with improved rate and cycle performance for lithium storage. *Carbon* 92:354–361

- [35] Guo R, Qi L, Mo Z, Wu Q, Yang S (2017) A new route to synthesize polyaniline-grafted carboxyl-functionalized graphene composite materials with excellent electrochemical performance. *Iran Polym J* 26:423–430
- [36] Ma J, Zhang X, Yan C, Tong Z, Inoue H (2008) Synthesis and characterization of a polyaniline/HTiNbO₅ lamellar hybrid nanocomposite. *J Mater Sci* 43:5534–5539. <https://doi.org/10.1007/s10853-008-2837-1>
- [37] Liu S, Liu X, Li Z, Yang S, Wang J (2011) Fabrication of free-standing graphene/polyaniline nanofibers composite paper via electrostatic adsorption for electrochemical supercapacitors. *New J Chem* 35:369–374
- [38] Zhang L, Zhang G, Liu C, Fan S (2012) High-density carbon nanotube buckypapers with superior transport and mechanical properties. *Nano Lett* 12:4848–4852
- [39] Xin G, Yao T, Sun H, Scott SM, Shao D, Wang G, Lian J (2015) Highly thermally conductive and mechanically strong graphene fibers. *Science* 349:1083–1087